Late Maastrichtian carbon isotope stratigraphy and cyclostratigraphy of the Newfoundland Margin (Site U1403, IODP Expedition 342)

Journal Item

Newsletters on Stratigraphy
Published online August 2017

PrePub Article

Late Maastrichtian carbon isotope stratigraphy and cyclostratigraphy of the Newfoundland Margin (Site U1403, IODP Leg 342)

Sietske J. Batenburg[1,3]*, Oliver Friedrich[3], Kazuyoshi Moriya[4], Silke Voigt[1], Cécile Cournède[5], Iris Moebius[3,6], Peter Blum[7], André Bornemann[8], Jens Fiebig[1], Takashi Hasegawa[4], Pincelli M. Hull[9], Richard D. Norris[10], Ursula Röhl[11], Philip F. Sexton[12], Thomas Westerhold[11], Paul A. Wilson[13], and the IODP Expedition 342 Scientists

With 7 figures and 2 tables

Abstract. Earth's climate during the Maastrichtian (latest Cretaceous) was punctuated by brief warming and cooling episodes, accompanied by perturbations of the global carbon cycle. Superimposed on a long-term cooling trend, the middle Maastrichtian is characterized by deep-sea warming and relatively high values of stable carbon-isotope ratios, followed by strong climatic variability towards the end of the Cretaceous. A lack of knowledge on the timing of climatic change inhibits our understanding of underlying causal mechanisms. We present an integrated stratigraphy from Integrated Ocean Drilling Program (IODP) Site U1403, providing an expanded deep ocean record from the North Atlantic (Expedition 342, Newfoundland Margin). Distinct sedimentary cyclicity suggests that orbital forcing played a major role in depositional processes, which is confirmed by statistical analyses of high resolution elemental data obtained by X-ray fluorescence (XRF) core scanning. Astronomical calibration reveals that the investigated interval encompasses seven 405-kyr cycles ($Ma_{405}1$ to $Ma_{405}7$) and spans the 2.8 Myr directly preceding the Cretaceous/Paleocene (K/Pg) boundary.

Authors' addresses:
[1] Institute of Geosciences, Goethe-University Frankfurt, Altenhöferallee 1, 60438 Frankfurt am Main, Germany.
[2] present address: Department of Earth Sciences, University of Oxford, South Parks Road, Oxford OX1 3AN, United Kingdom.
[3] Institute of Earth Sciences, Ruprecht-Karls-University Heidelberg, Im Neuenheimer Feld 234–236, 69120 Heidelberg, Germany.
[4] School of Natural Sciences and Technology, Kanazawa University, Kakuma-machi, Kanazawa, Ishikawa 920-1192, Japan.
[5] CEREGE, Université Aix-Marseille, Europole de l'Arbois BP 80 1, 13545 Aix en Provence, France.
[6] present address: Lamont-Doherty Earth Observatory, Columbia University, 61 Route 9W, Palisades NY 10964, USA.
[7] Integrated Ocean Drilling Program, Texas A&M, 1000 Discovery Drive, College Station, TX 77845-9547, USA.
[8] Bundesanstalt für Geowissenschaften und Rohstoffe, Stilleweg 2, 30655 Hannover, Germany.
[9] Department of Geology and Geophysics, Yale University, 210 Whitney Ave, New Haven, CT 06511, USA.
[10] Scripps Institution of Oceanography, University of California San Diego, 9500 Gilman Drive, La Jolla, CA 92093-0244, USA.
[11] MARUM-Center for Marine Environmental Sciences, University of Bremen, Leobener Strasse 8, 28359 Bremen, Germany.
[12] School of Environment, Earth & Ecosystem Sciences, The Open University, Walton Hall, Milton Keynes MK7 6AA, UK.
[13] National Oceanography Centre Southampton, University of Southampton, Waterfront Campus, European Way, Southampton SO14 3ZH, UK.
* Corresponding author: Sietske J. Batenburg, Department of Earth Sciences, University of Oxford, South Parks Road, Oxford OX1 3AN, United Kingdom. sbatenburg@gmail.com

www.borntraeger-cramer.de
DOI: 10.1127/nos/2017/0398
0078-0421/2017/0398 $ 4.00

A high-resolution carbon-isotope record from bulk carbonates allows us to identify global trends in the late Maastrichtian carbon cycle. Low-amplitude variations (up to 0.4‰) in carbon isotopes at Site U1403 match similar scale variability in records from Tethyan and Pacific open-ocean sites. Comparison between Site U1403 and the hemipelagic restricted basin of the Zumaia section (northern Spain), with its own well-established independent cyclostratigraphic framework, is more complex. Whereas the pre-K/Pg oscillations and the negative values of the Mid-Maastrichtian Event (MME) can be readily discerned in both the Zumaia and U1403 records, patterns diverge during a ~1 Myr period in the late Maastrichtian (67.8–66.8 Ma), with Site U1403 more reliably reflecting global carbon cycling. Our new carbon isotope record and cyclostratigraphy offer promise for Site U1403 to serve as a future reference section for high-resolution studies of late Maastrichtian paleoclimatic change.

Key words. integrated stratigraphy, paleoclimatology, Maastrichtian, astronomical climate forcing, carbon isotopes, Ocean Drilling Program Site U1403 (Newfoundland)

1. Introduction

Following the high temperatures of the mid-Cretaceous greenhouse (e.g. in tropical Atlantic records generated by Wilson et al. 2002, Forster et al. 2007, Bornemann et al. 2008 and Friedrich et al. 2008), the latest Cretaceous is characterized by long-term climate cooling until the late Campanian to Maastrichtian (e.g. in compilations by Clarke and Jenkyns 1999, Huber et al. 2002, Friedrich et al. 2012). Superimposed on this long-term trend are several short-term cooling pulses with the most pronounced episode occurring across the Campanian-Maastrichtian boundary, the globally recognized Campanian–Maastrichtian Boundary Event (Voigt et al. 2010, CMBE). The CMBE is characterized by distinct changes in stable oxygen and carbon isotope records, indicating deep-water cooling and changing rates of global organic carbon burial (e.g., Barrera et al. 1997, Frank and Arthur 1999, Barrera and Savin 1999, Friedrich et al. 2004, 2009, Frank et al. 2005, Friedrich and Hemleben 2007, Voigt et al. 2012, Jung et al. 2013). Shortly after the CMBE, the Mid-Maastrichtian Event (MME; recognized in the North Atlantic by MacLeod et al. 1996) marks a time of deep-sea warming (e.g. in the Tropical Pacific; Jung et al. 2013) and an inoceramid extinction event in numerous open-ocean sites (e.g., MacLeod 1994, MacLeod et al. 1996). The last 400 kyr of the Cretaceous are characterized by a strong oscillation in carbon isotope records (Voigt et al. 2012), accompanied by a pulse of global warming, as recognized in bulk carbonate oxygen isotope records and foraminiferal and nannofossil assemblages (Barrera 1994, Li and Keller 1998, Thibault et al. 2007, 2016b), as well as in terrestrial records (Wilf et al. 2003).

Although the CMBE, the MME, and the climatic instability near the end of the Cretaceous have been studied extensively (Thibault et al. 2007, Jung et al. 2013, and references therein), the causal mechanisms triggering the events are still poorly understood due in part to weak constraints on their timing. The low temporal resolution of Maastrichtian biozonation schemes and pronounced biotic provincialism complicate correlation further. This provincialism is related to the latest Cretaceous climate cooling which resulted in the formation of three main provinces (Tethyan, Boreal, and Austral, e.g., Huber and Watkins 1992, Premoli Silva and Sliter 1994, Burnett 1998, Lees 2002, Lees and Bown 2005). To overcome the limitations of poorly resolved age models and biotic provincialism, high-resolution carbon isotope curves ($\delta^{13}C$ records) have recently been used for detailed stratigraphic correlation of Maastrichtian sections from a variety of depositional settings (e.g., Voigt et al. 2010, 2012, Batenburg et al. 2012, Jung et al. 2012, Thibault et al. 2012a, b). Successful correlation of carbon isotope stratigraphies from the European shelf seas with datasets derived from deep-sea sediments in the tropical Pacific Ocean demonstrated the utility and accuracy of this approach (Voigt et al. 2010, 2012).

An astronomical age scale has recently been established for the Maastrichtian (Husson et al. 2011, Batenburg et al. 2012, 2014, Thibault et al. 2012a), allowing for more precise reconstruction of the duration of Maastrichtian events and their relative timing between different regions. However, these new timescale developments are currently based on physical property data from either marginal hemipelagic sections (northern Spain; Batenburg et al. 2012, 2014), correlated pelagic sites (Indian Ocean, equatorial and South Atlantic Ocean; Husson et al. 2011) or sites with incomplete recovery (Indian Ocean Site 762C; Thibault et al. 2012a) and require validation from continuous pelagic successions with diagenetically robust geologic data.

Here, we present a new, high-resolution carbon isotope dataset from Integrated Ocean Drilling Program (IODP) Site U1403 that records carbon-cycle fluctuations in the late Maastrichtian North Atlantic near Newfoundland. Site U1403 provides an exceptional archive of rhythmic, continuous sedimentation in the northernmost high-resolution Maastrichtian deep-ocean record to date. Site U1403 is in a particularly useful location because it would have likely lain in the pathway of the Northern Component water mass suggested to have formed an important component of deep water in the Late Cretaceous Atlantic Ocean (e. g., MacLeod et al. 2011, Robinson and Vance 2012, Voigt et al. 2013).

We find a close correspondence between the carbon isotope dataset of Site U1403 and other open ocean carbon isotope records from the equatorial Pacific Ocean (ODP Hole 1210B on Shatsky Rise) and the Tethys Ocean (the Gubbio section in the Umbria–Marche Basin, Italy). Using high-resolution X-ray fluorescence (XRF) core scanning data, we present an orbital timescale for the Upper Maastrichtian interval of Site U1403 through the identification of hierarchical Milankovitch cycles. The orbital timescale presented in this study provides independent support of the carbon isotope stratigraphy. However, marked differences are observed when comparing Site U1403 to the high-resolution chemostratigraphic framework of the Zumaia section (northern Spain; Batenburg et al. 2012, 2014). The divergence in $\delta^{13}C$ records between these two sites allows us to disentangle global versus regional influences on carbon cycling and supports the utility of Site U1403 as an open ocean reference site for the latest Cretaceous.

2. Materials and Methods

2.1 Geological setting of Site U1403

Integrated Ocean Drilling Program Site U1403 (39° 56.60′ N, 51° 48.20′ W) is located at the foot of the J-Anomaly Ridge off Newfoundland (Fig. 1). Site U1403 was drilled in 2012 during IODP Expedition 342 at a present-day water depth of 4949 m and is the deepest site drilled in the Newfoundland depth transect (Expedition 342 Scientists 2012).

Maastrichtian-aged sediments at Site U1403 are nannofossil chalks that show subtle, decimeter-scale, rhythmic color variations between pale yellow and very pale brown (lithological Unit Vb of Site U1403; see Expedition 342 Scientists (2012) for a detailed description of lithostratigraphic units). Calcium carbonate content of Maastrichtian sediments ranges from 35 to 80 wt% (Norris et al. 2014), suggesting that Site U1403 was above the CCD during the Late Cretaceous.

2.2 Stable isotopes

Site U1403 has been sampled at a resolution of ~ 10 cm for stable carbon- and oxygen-isotope analyses on bulk carbonates. A total of 253 samples were taken from cores 26 to 28 of Hole A and cores 28 to 32 of Hole B, spanning 247.68–296.23 m core composite depth below sea floor (rCCSF; Fig. 2) Bulk samples were dried, ground, and alternatingly analyzed using either a Finnigan MAT 253 coupled online to a Gasbench II at Goethe-University Frankfurt (Germany) or a Finnigan Delta V Advantage coupled with Gasbench II at Kanazawa-University (Japan; for details see Moriya et al. 2012). All isotope values are reported in ‰ relative to the Vienna Peedee belemnite standard

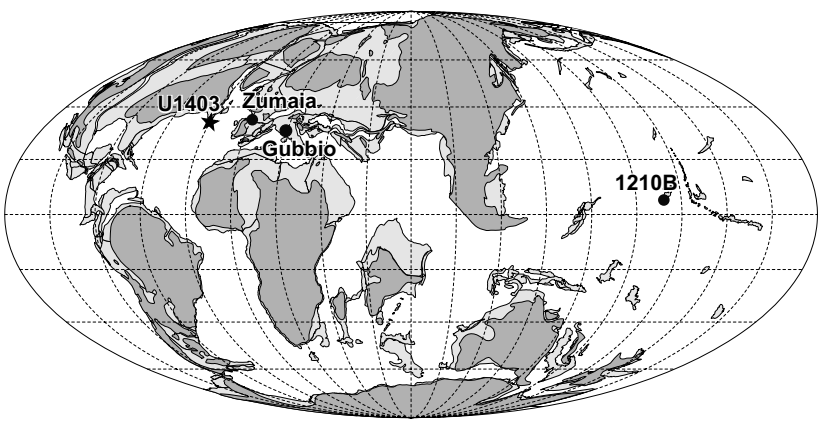

Fig. 1. Paleogeographic reconstruction for the Maastrichtian (70 Ma) reconstruction (after Voigt et al. 2012; based on www.odsn.de; Hay et al., 1999) showing locations of sites discussed.

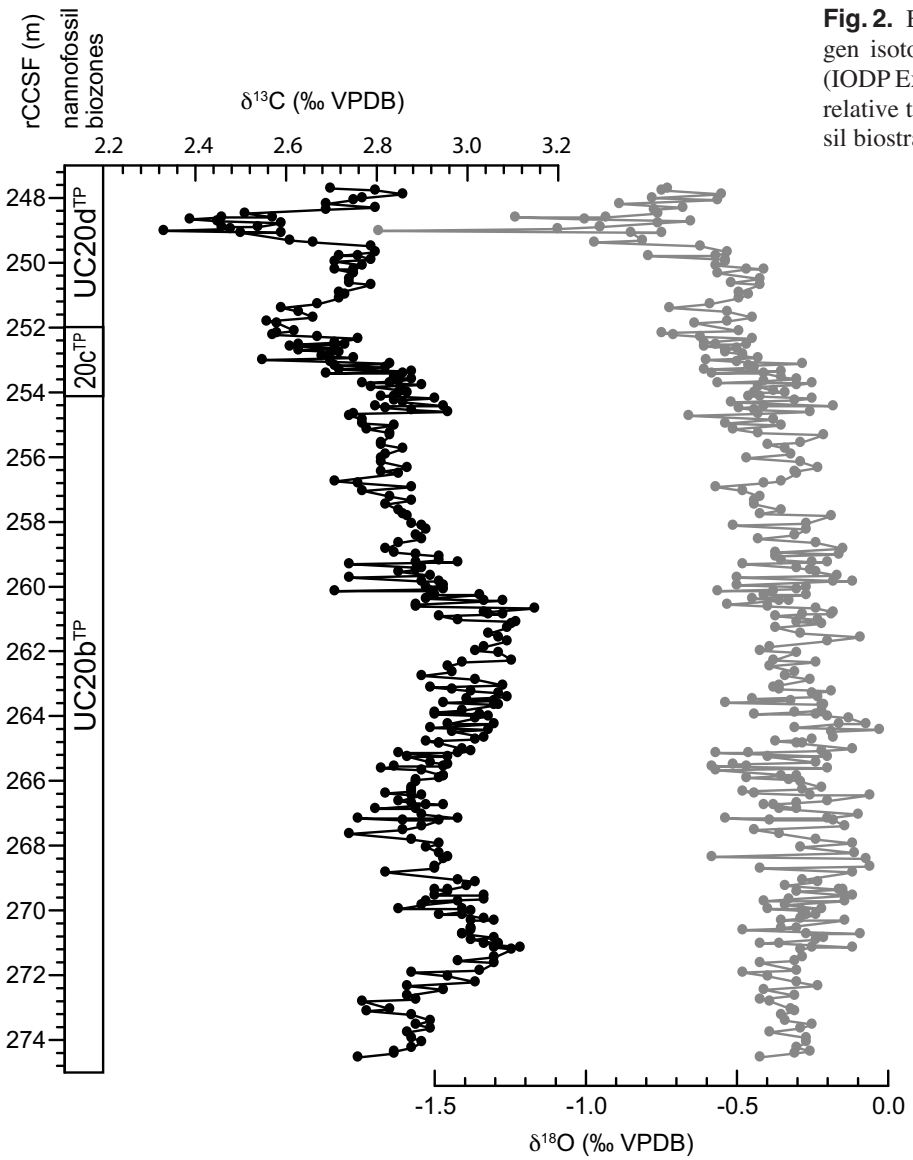

Fig. 2. Bulk-carbonate carbon and oxygen isotope data from IODP Site U1403 (IODP Expedition 342) against rCCSF and relative to shipboard calcareous nannofossil biostratigraphy (Norris et al. 2014).

(VPDB). For both systems, the analytical precision of replicates of standard measurements was better than 0.06 and 0.08‰ for carbon and oxygen, respectively. Duplicate measurement of the same sample on both machines resulted in no discernable difference outside of analytical error.

2.3 XRF scanning

The Maastrichtian interval of Site U1403 was analyzed by XRF scanning (X-Ray Fluorescence) on the surface of the core archive-halves in the MARUM XRF Core Scanner Lab, University of Bremen, Germany. The AVAATECH instrument, serial no. 11, with an Oxford Instruments 100W Neptune Rh X-Ray tube and a Canberra X-PIPS Silicon Drift Detector (SDD, Model SXD 15C-150-500) was set to a step-size of 15 mm, a slit down-core of 10 mm, and a slit cross-core of 12 mm. A first run collected data at 10 kV, 1.0 mA, for 20 s, and a second run at 50 kV, 0.2 mA, for 20 s. The data were processed with WIN AXIL batch software using a 10kV_Cl-Rh model and a 50kV model, respectively. Outliers, likely resulting from uneven core surfaces or micro cracks, were removed and not shown in Figure 3.

2.4 Time series analyses and astronomical calibration

To reduce noise, the natural logarithm of Fe over Ca was selected for further analyses (ln(Fe/Ca)), following the approach of Weltje and Tjalingii (2008), as

well as the shipboard magnetic susceptibility data (WRMSL-MS, Expedition 342 scientists 2012). The data were evenly interpolated and periodicities larger than 5 m and 1 Myr were removed as these periodicities are too long to be reliably detected in the upper Maastrichtian elemental and physical property data. Periodicities were investigated using a wavelet application for Matlab (Grinsted et al. 2004) in the depth and time domains.

In the elemental records, particularly in Si, Fe, and ln(Fe/Ca), a sharp peak occurs between 265.60 and 265.85 m rCCSF. In addition, a high-variability interval is observed directly below the K/Pg boundary from 249 to 247 mcd. The data records were cut at these levels to avoid complications from potential changes in sedimentation rate and spectral analyses with Redfit 3.8 (Schulz and Mudelsee 2002) were performed on both the partial records as well as on the complete data series (Figs. 4 and 5). Based on the detected spectral peaks (see Sect. 4), band-pass filters were applied using AnalySeries (Paillard et al. 1996). The filters were centered at 4.5 m (whole record), 4.3 m (upper partial record) and 3.3 m (lower partial record) for ln(Fe/Ca), and at 4.4 m for magnetic susceptibility (whole record), with a bandwidth of approximately one third of the center frequency (Fig. 4, see caption for filter details).

Consecutive minima in the ln(Fe/Ca) record that occur near minima in the band-pass filters (Fig. 4) were calibrated to successive minima in the 405-kyr component of eccentricity from the new La2011 (nominal) solution (Laskar et al. 2011) based on a 405-kyr band-pass filter with a bandwidth of 300–623 kyr. The stable 405-kyr periodicity of eccentricity is the only reliable tuning target that can be reconstructed beyond ~52 Ma (Laskar et al. 2011).

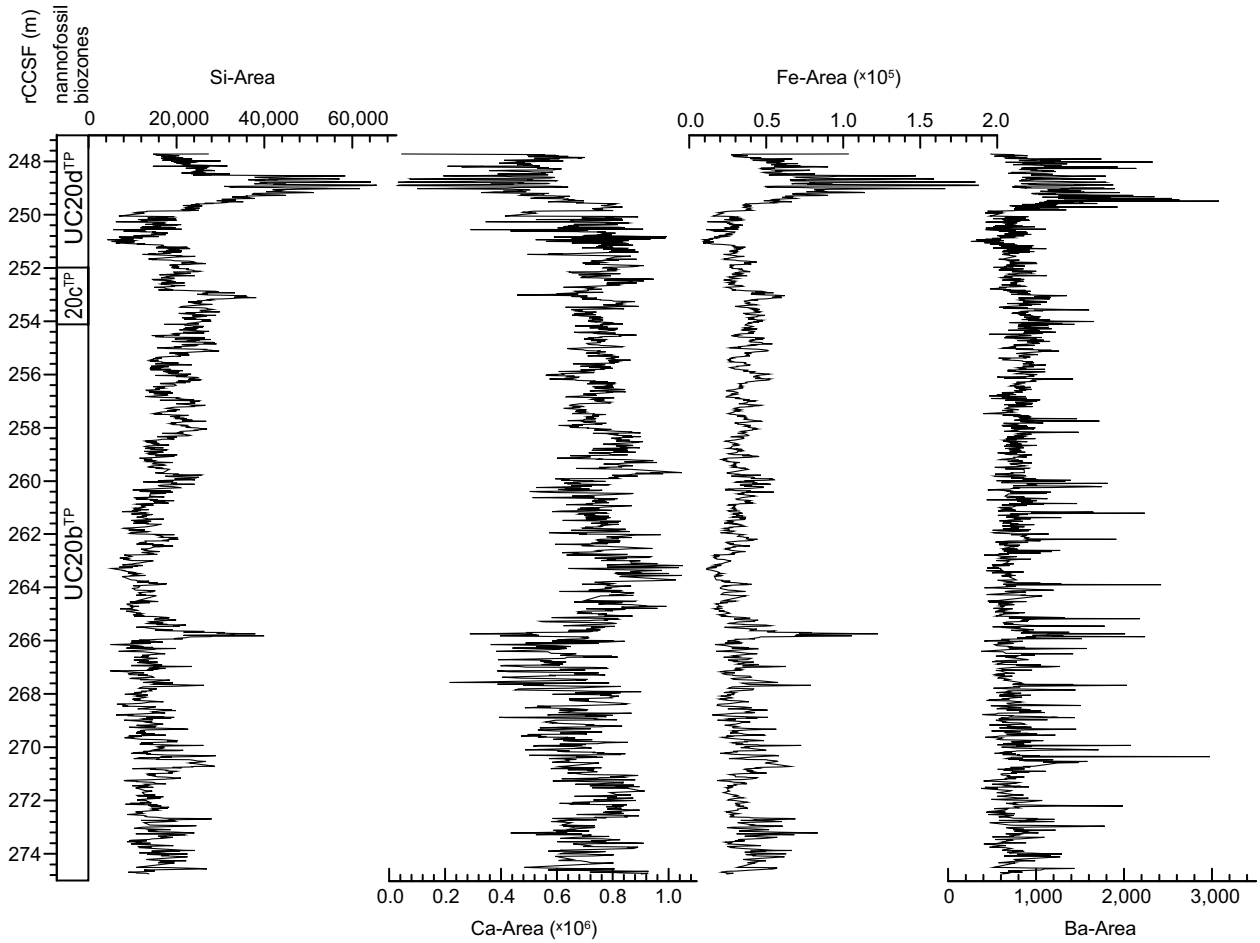

Fig. 3. High-resolution XRF core-scanning silica, calcium, iron and barium elemental intensities from IODP Site U1403 (IODP Expedition 342) against rCCSF and relative to shipboard calcareous nannofossil biostratigraphy (Norris et al. 2014).

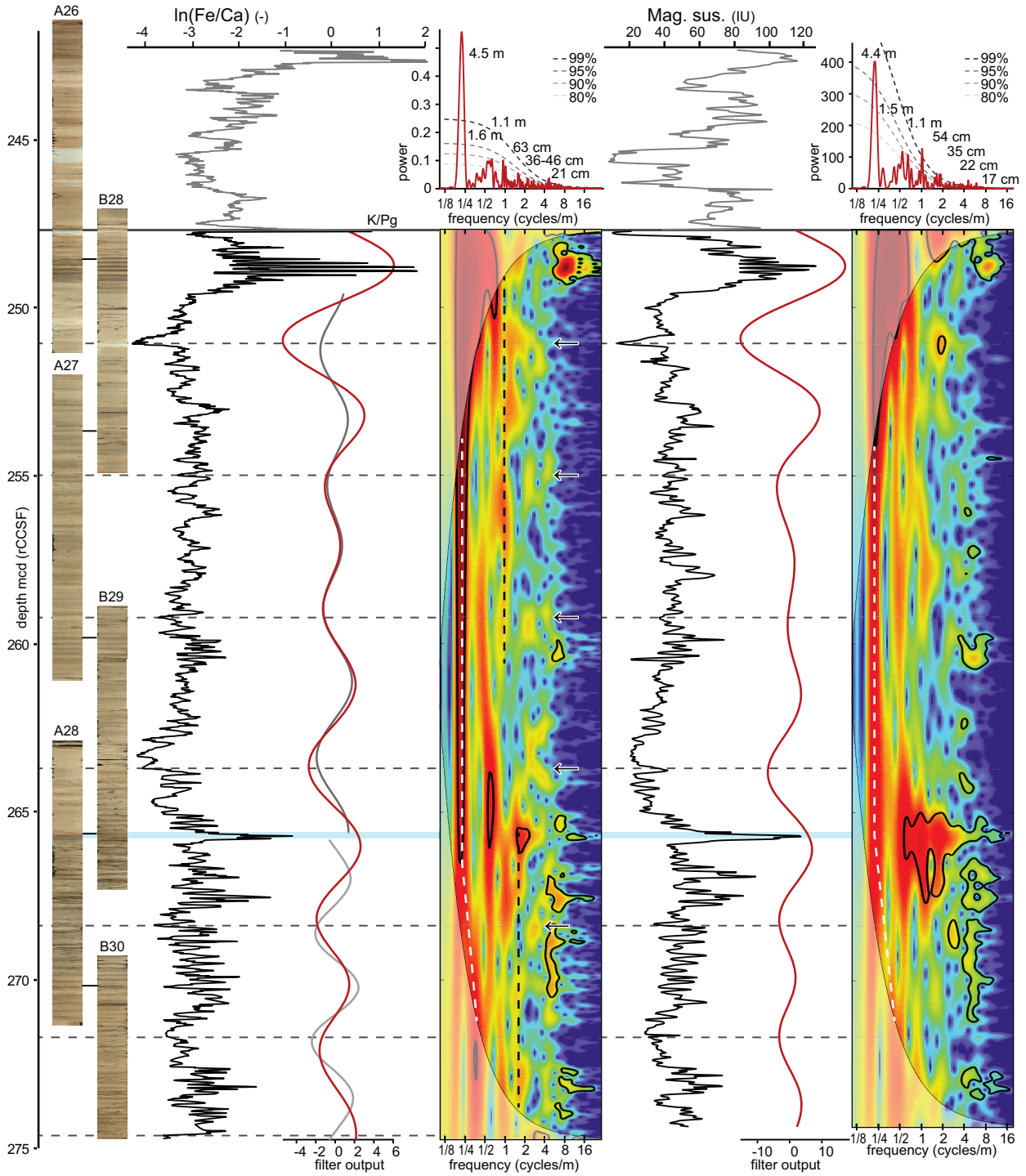

Fig. 4. Time series analyses of the natural logarithm of the ratio of Fe and Ca counts (ln(Fe/Ca)), obtained by XRF scanning of the Maastrichtian interval of U1403, and the magnetic susceptibility (shipboard data, instrument units). From left to right: joined core photographs with splice tie-points (black bars), ln(Fe/Ca) (left) and magnetic susceptibility (right) in the depth domain, flanked by band-pass filters, wavelet analyses and Redfit power spectra. For ln(Fe/Ca), the band-pass filter over the whole record is indicated in red and centered at 4.5 m (bandwidth 3.4–6.8 m). The band-pass filters over the partial records are centered at 4.2 m (bandwidth 3.1–6.3 m) for the upper part (dark grey) and 3.3 m (bandwidth 2.5–5.0 m) for the lower part (light grey). For magnetic susceptibility, the band-pass filter over the whole record, in dark red, is centered at 4.4 m (bandwidth 3.3–6.7 m). Blue shading indicates the interval between 265.60 and 265.85 m rCCSF, where the records are cut. Black arrows within the wavelet analyses panel of ln(Fe/Ca) indicate periodic amplitude amplifications in the frequency band of 36–46 cm. Dark grey dashed lines indicate the stratigraphic positions of minima in the ln(Fe/Ca) record that occur within minima in the band-pass filters, and are used as tie-points for the age model (Table 2).

Table 1 Adjusted splice table for the Maastrichtian interval of Site U1403. A 25-cm shift is applied to the shaded values.

Hole	Core	Sect.	Level (cm)	m CSF-A	m rCCSF		Hole	Core	Sect.	Level (cm)	m CSF-A	m rCCSF
A	27	6	48.50	232.19	259.88	TIE	B	29	1	91	227.21	259.88
B	29	5	91.00	232.96	265.63	TIE	A	28	2	119.4	236.594	265.63
A	28	5	134.30	240.993	270.03	TIE	B	30	1	89	236.89	270.03
B	30	4	115.00	241.4	274.54	APPEND	B	31	1	2.5	245.725	279.84
B	31	CC	71.30	251.873	285.98	APPEND	B	32	1	2.5	255.425	290.51
B	32	5	88.60	261.736	296.82							

3. Results and discussion

3.1 XRF scanning results and splice correction of Site U1403

Based on the XRF scanning results, a small correction of the shipboard splice is suggested. Specifically, we shift the tie-point in Hole A, Core 27, Section 6, at 23.50 cm down-core by 25 cm, from an original depth of 259.63 m CCSF to a revised depth of 259.88 m rCCSF (revised CCSF). All consecutive tie-points were adjusted accordingly and provided in Table 1. All depths beyond 259.63 m rCCSF mentioned in this manuscript are on the revised CCSF scale (Table 1). The 25-cm shift leads to a better matching of peaks in, among others, the Fe records of Holes A and B with high signal-to-noise-ratio from 259 to 261 m rCCSF. The revised splice also results in better agreement across holes in magnetic susceptibility and color reflectance data, although these data types are more variable (Expedition 342 Scientists 2012).

The elemental records can be divided in two main groups (data on www.pangaea.de). The elements Al, Si, K, Ti, Mn, Fe, and Zr are anti-correlated to carbonate-phase elements Ca and Sr (Fig. 3). The element Ba (reported as total Ba analyzed) displays a third type of behavior and is characterized by relatively stable background values interrupted by intervals with high-frequency, sharp peaks (Fig. 3). The ln(Fe/Ca) record shows a sharp peak between 265.60 and 265.82 m rCCSF, indicated by blue shading in Figure 4. This peak coincides with a marked change in the visual appearance of the cores, with closely spaced dark bands occurring below 265.60 m rCCSF, and wider bands of lighter color occurring above (core images in left panel of Fig. 4). These bands occur in groups or bundles throughout the studied interval.

3.2 Time series analyses and cyclostratigraphy

The magnetic susceptibility and elemental records show variability on different spatial scales, such as a marked ~20 cm variability in the two meters below the K/Pg boundary and a ~1 m variability between 255 and 259 m CCSF. The spectra of the ln(Fe/Ca) and magnetic susceptibility data-sets display many spectral peaks when the complete records are analyzed (top panels Fig. 4). Main periodicities in the ln(Fe/Ca) record, above 99% confidence, are at 4.5 m, 21–22 cm and around 17 cm. Other prominent peaks, above 90% confidence, occur at 1.6 m, 1.1 m, 63 cm, 46 cm, 36 cm and 27 cm. For magnetic susceptibility, the main periodicities, above 99% confidence, are at 4.4 m, 1.1 m, 54–60 cm, 35 cm, 26–28 cm, 22 cm, 20 cm and around 17 cm. The numerous peaks in the power spectrum of the whole data series may be due to changes in sedimentation rate through the succession.

The partial records resulting from cutting the records at 249.56 m, 265.60 m and 265.85 m rCCSF provide cleaner spectra (Fig. 5). The periodicities above 99% confidence in the upper partial record of ln(Fe/Ca) are at 44 cm, 36 cm, 26 cm, 21–22 cm and 16–17 cm, and above 90% confidence, periodicities of 4.2 m and 1.0 m are detected. For the upper partial record of magnetic susceptibility, main periodicities occur at 25–29 cm, 22 cm, 20 cm and 16–18 cm (above 99% confidence), and other periodicities at 95 cm, 43 cm (above 95% confidence) and at 2.1 m and 36 cm (above 90% confidence). The lower partial

record of ln(Fe/Ca) has main periodicities at 22 cm and 15 cm (above 99 % confidence), and other prominent periodicities at 3.3 m and 17 cm (above 95 % confidence). The lower partial record of magnetic susceptibility shows dominant periodicities around 20–22 cm (above 99 % confidence), and other prominent periodicities at 3 m, 53 cm and 35 cm (above 90 % confidence). For completeness, the spectral analyses of the records cut only at 249.56 m are also shown (Fig. 5, lower panels).

The strong periodicities in the upper part of the ln(Fe/Ca) and magnetic susceptibility records, at 4.2 m, 1 m, 44 cm, 36 cm, and 21–22 cm, have a ratio near that of the main periodicities of the orbital parameters of eccentricity-modulated precession and obliquity (20 : 5 : 2 : 1, formed by the ratio of the 405 kyr, 100 kyr, 41 kyr and 22 kyr components). In the upper part of the record, a periodicity of 2.1 m is detected, which would correspond to a periodicity of about 200 kyr. Such a peak can occur by interference of, and non-linear sedimentary responses to, the 405 kyr and 100 kyr periodicities of eccentricity-modulated precession (Liebrand et al. 2017). Alternatively, a peak at 200 kyr can occur as a result of the strong expression of every second

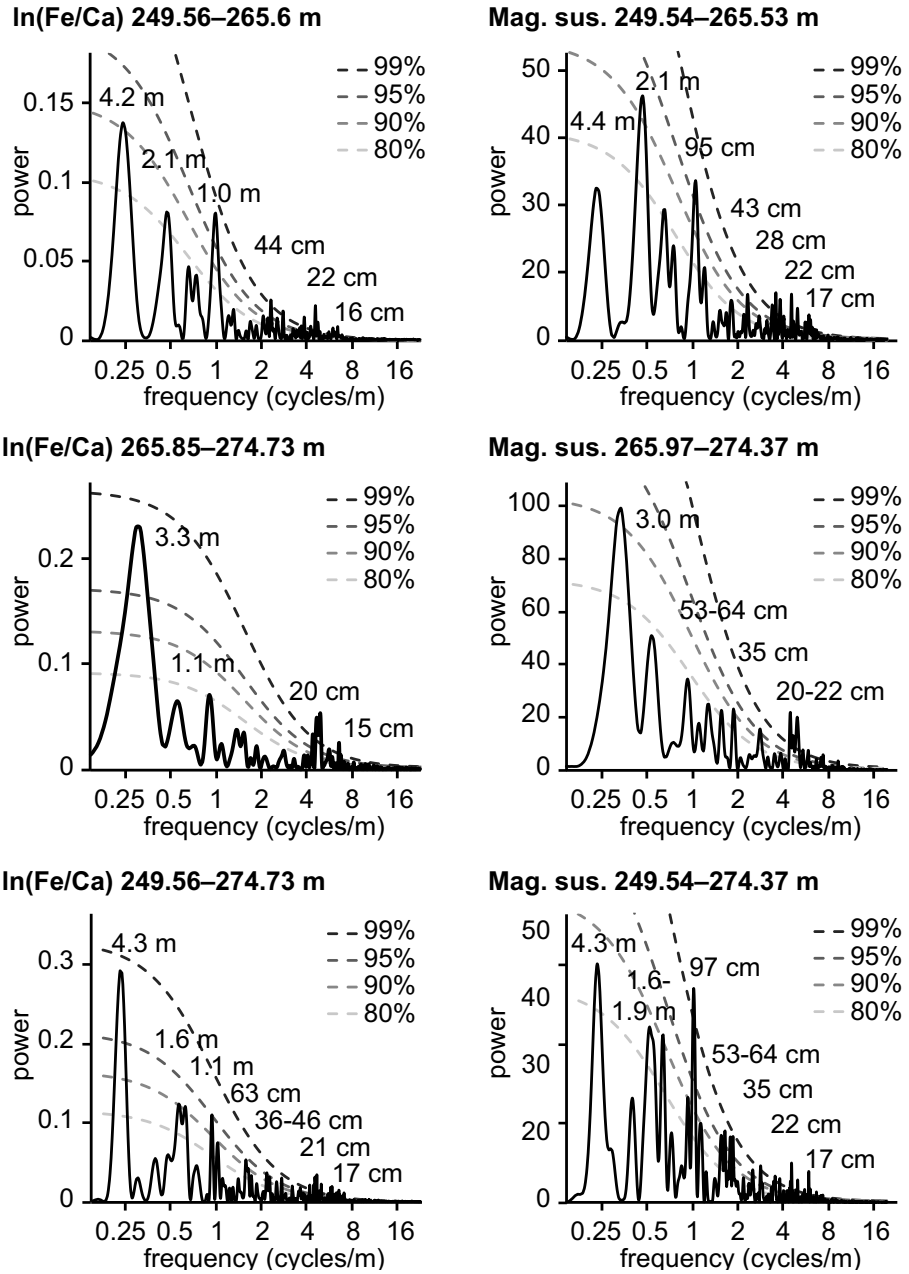

Fig. 5. Redfit power spectra of the partial records of ln(Fe/Ca) (left) and magnetic susceptibility (right). Top panel: the upper interval between the peak at 265.6 m and the variability below the K/Pg boundary, starting at 249.56 m; middle panel: the lower interval from the peak at 265.85 m downwards; bottom panel: the interval from the main variability below the K/Pg, starting at 249.56 m, downwards.

~ 100 kyr cycle. This can be due to variations in climate and sedimentation that are not related to Milankovitch forcing, or it can be a property of the astronomical forcing parameters related to very long (Myr) periodicities of eccentricity, as can be observed in long-term reconstructions of eccentricity (Laskar et al. 2011). In the lower part of the record, periodicities at 3.3 and 3.0 m, 64 cm, 22 cm and 15 cm also seem to reflect the hierarchical pattern of the main periodicities of eccentricity-modulated precession and obliquity (20 : 5 : 2 : 1), albeit less clearly due to the shorter length of the lower partial record. The shift in periodicities is likely caused by an increase in sedimentation rate at 265.60 m rCCSF, a hypothesis which is supported by the increase in the spacing of dark bands (Fig. 4).

Establishing a cyclostratigraphic age-model requires resolving the phase relationship between the variability in the data records and the 405-kyr periodicity of eccentricity-modulated precession. During overall maxima of Fe and minima of Ca and corresponding maxima of ln(Fe/Ca), the respective records are characterized by high variability (Fig. 4). This pattern likely reflects the sedimentary response to eccentricity-modulated precession, with high variability caused by large amplitude of the precessional forcing during eccentricity maxima. The observed rhythmic pattern reflects some combination of the three factors influencing sediment composition: carbonate productivity; carbonate content dilution by siliciclastic terrigenous input; and carbonate dissolution. Maxima in Fe counts coincide with minima in Ca counts (high ln(Fe/Ca)) and can be interpreted to reflect increasing terrigenous input, decreased carbonate production, increased carbonate dissolution, or some combination of two to three of the above. We hypothesize that our data reflect highest terrigenous input and/or lowest carbonate production in times of maximal eccentricity. Increased terrigenous input during eccentricity maxima could result from more runoff due to an intensified hydrological cycle. Increased variability in runoff during eccentricity maxima could reflect a corresponding increase in influence of precessional forcing on the hydrological regime. In this scenario, minima of Ca would primarily reflect dilution by terrigenous material. In contrast, the dark bands observed directly below the K/Pg boundary (see core pictures in Fig. 4) may reflect local short-lived dissolution events that led to additional Fe enrichment and Ca depletion, as is observed in other deep sea sites (Henehan et al. 2016).

Based on the above-mentioned sedimentary response to eccentricity-modulated precession, minima in the ln(Fe/Ca) record that occur near minima in the 4.5 m, 4.4 m and 3.3 m band-pass filters are assigned the ages of minima in the 405-kyr component of eccentricity from the La2011 solution (Laskar et al. 2011) (Table 2). This interpretation is supported by the occurrence of increased amplitude of 36–46 cm periodicities at five such levels, which likely correspond to more prominent obliquity forcing during 405-kyr eccentricity minima. Our astronomical calibration is anchored to a K/Pg boundary age of 66.04 Ma based on new bentonite ages from coals near the K/Pg boundary (Renne et al. 2013). After assigning ages to the consecutive 405-kyr minima, the main periodicities of the calibrated ln(Fe/Ca) record are at 404, 143, 24 and 22 kyr (above 99 % confidence), with other periodicities (above 90 % confidence) at 96, 85, 51 and 38 kyr. For the calibrated magnetic susceptibility record, main periodicities are at 417, 85, 46, 34, 24 and 19 kyr, with other periodicities at 143 and 97 kyr (Fig. 6). These periodicities broadly correspond to the periodicities of obliquity and eccentricity-modulated precession, and their combination tones, and display a regular behavior throughout the record (wavelet panels, Fig. 6).

The investigated interval of Site U1403 encompasses seven 405-kyr cycles in total ($Ma_{405}1$ to $Ma_{405}7$, Husson et al. 2011 following the nomenclature of Westerhold et al. 2008; Fig. 6) and spans 2.8 Myr (68.8 to 66.04 Ma). The regular sedimentary cyclicity highlights the potential of Site U1403 to serve as a latest Maastrichtian reference section in the Atlantic Ocean. Site U1403 provides the possibility to investigate the timing and duration of underlying causes and trigger mechanisms of climatic and oceanographic events and fluctuations like the MME or the K/Pg boundary as well as the time interval in-between.

Table 2 Tie-points for constructing the orbital age model and resulting linear sedimentation rates.

Depth mcd (rCCSF)	Age (Ma)	Sed. Rate (cm/kyr)
247.700	66.04	
251.040	66.374	1.00
254.960	66.782	0.96
259.205	67.192	1.04
263.695	67.585	1.14
268.365	67.986	1.16
271.680	68.383	0.84
274.635	68.787	0.73
275.000	68.837	0.73

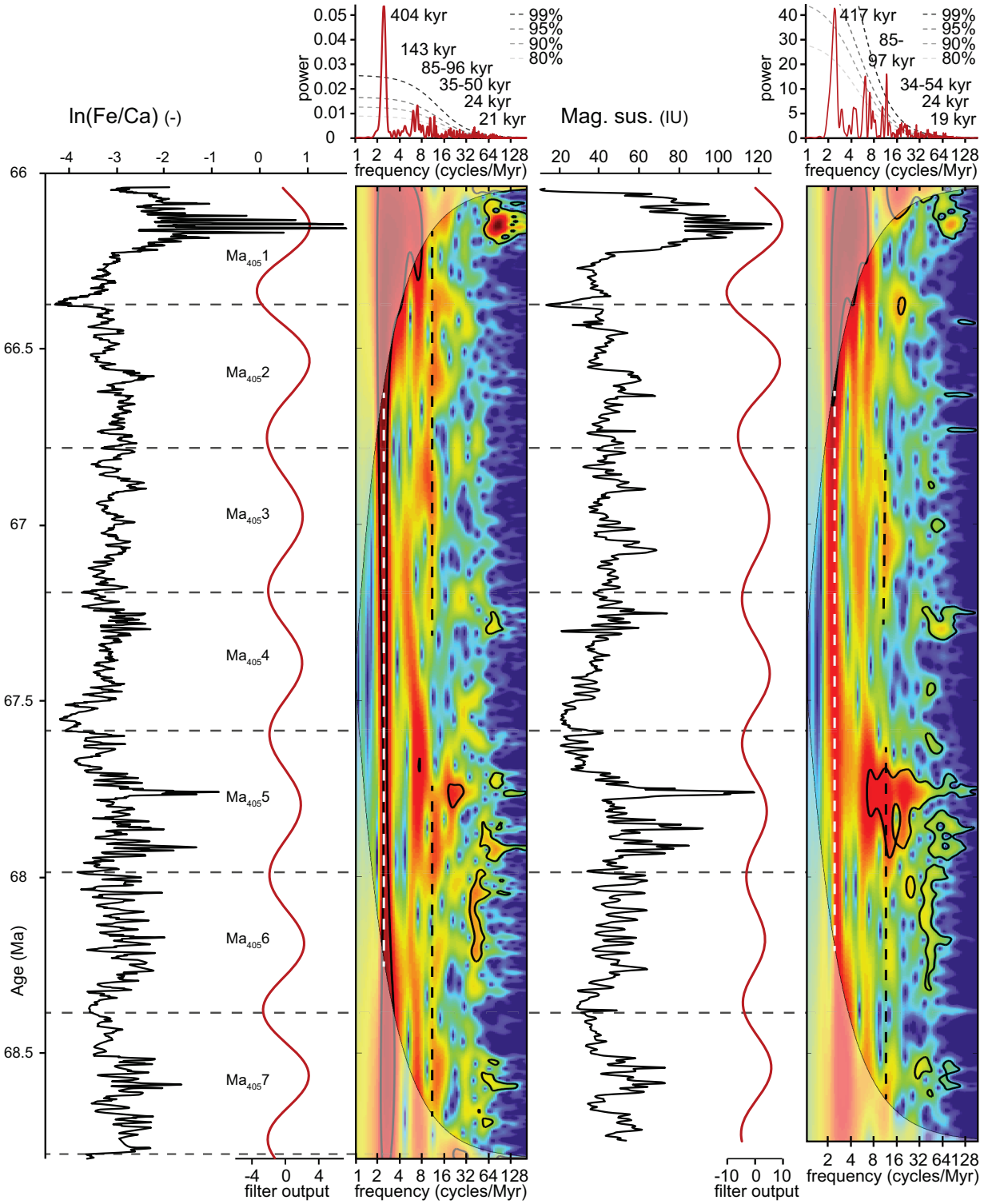

Fig. 6. Time series analyses of the ln(Fe/Ca) and magnetic susceptibility records calibrated to the 405-kyr component of eccentricity. Left: the ln(Fe/Ca) record in the time domain, flanked by a band-pass filter centered at 404 kyr (bandwidth 302–612 kyr), and wavelet analyses, topped by a Redfit power spectrum. The curved grayscale lines indicate the 99 %, 95 %, 90 % and 80 % confidence levels, from the uppermost to the lowermost, respectively. Right: the same for the magnetic susceptibility record, with a band-pass filter centered at 417 kyr (bandwidth 313–627 kyr). Dark grey dashed lines indicate the positions of minima in the ln(Fe/Ca) record that are used as tie-points in the age model. Ma_{405} numbers indicate the 405-kyr cycle from the K/Pg boundary back in time.

3.3 Stable oxygen isotope signal

Site U1403 nannofossil oozes consist mainly of coccoliths and benthic and planktic foraminifera (Expedition 342 Scientists 2012). Bulk oxygen isotope values therefore predominantly represent a surface-water signal. However, the $\delta^{18}O$-composition of bulk carbonate can be significantly altered by diagenetic processes like low-temperature exchange with pore fluids or burial diagenesis (e.g., Marshall 1992, Schrag et al. 1995). Therefore, we refrain from calculating absolute temperatures based on oxygen isotope values. Even so, variations in bulk oxygen isotope records are often considered to reflect relative changes in temperature (e.g., Jenkyns et al. 1994, Voigt and Wiese 2000, Friedrich et al. 2003), although lithology-related changes in stable oxygen isotopes can also occur. A lithology-related driver, such as differences in porosity or pore-fluid composition, would result in a $\delta^{18}O$ signal that mainly reflects fluctuations of the carbonate content of the analyzed sediments (Thierstein and Roth 1991). At Site U1403, a comparison between the $\delta^{18}O$ values with the Ca counts from XRF scanning show no correlation between these two factors (r^2 of 0.13). Also, individual negative peaks in the $\delta^{18}O$ record (values lower than 0.9‰) in the interval below the K/Pg boundary (246.56–247.7 m CCSF) show no consistent relationship with peak values of ln(Fe/Ca) (above –1.7 in a range of –3 to 2), that may represent dissolution events, arguing for $\delta^{18}O$ fluctuations independent of lithological changes.

The bulk carbonate oxygen isotope record from Site U1403 is characterized by relatively stable values between 253 and 275 m rCCSF of between 0 and –0.6‰ (Fig. 2). Above 253 m CCSF, $\delta^{18}O$ values decrease slightly, followed by a pronounced negative excursion between 249 and 248 m CCSF with minimum values of –1.5‰ within nannofossil zone UC20d^{TP} (Fig. 2). This decrease in oxygen isotope values suggests a significant increase in surface-water temperatures directly preceding the K/Pg boundary, as has been described in previous studies based on planktic foraminifera (e.g., Barrera 1994, Li and Keller 1998) and bulk stable isotope records (e.g., Thibault et al. 2016a).

3.4 Carbon isotope stratigraphy and global correlation

Carbon isotope values of carbonates are less prone to diagenetic alterations than oxygen isotope values (e.g., Anderson and Arthur 1983, Marshall 1992) and can be reliable recorders of changes in the global carbon cycle (e.g., Weissert et al. 2008, Kirtland-Turner et al. 2014). Especially for Cretaceous pelagic carbonate successions, carbon isotope stratigraphy has been successfully used for stratigraphic correlation on a global scale and across different depositional settings (e.g., Scholle and Arthur 1980, Jenkyns et al. 1994, Voigt et al. 2010, 2012, Jung et al. 2012, Thibault et al. 2012a, b).

The bulk carbon isotope record of Site U1403 shows variability on long and short timescales. While $\delta^{13}C$ values increase in the lower half of the record (275 to 260 m rCCSF, Fig. 2) to maximum values of 3.15‰, they decrease towards the top of the studied interval, resulting in minimum values of 2.3‰. The pattern of $\delta^{13}C$ values found in Site U1403 is similar to trends in bulk carbonate $\delta^{13}C$ values from the open-ocean settings of ODP Hole 1210B on Shatsky Rise in the equatorial Pacific (Jung et al. 2012) and Gubbio in the Umbria–Marche Basin of Italy (Voigt et al. 2012), as well as from the hemipelagic Zumaia section in N-Spain (Batenburg et al. 2012; Fig. 7). The records of Zumaia, 1210B and Gubbio have been correlated using four tie-points (Fig. 7): 1) the K/Pg boundary; 2) the $\delta^{13}C$ minimum below the C29r/C30n boundary, equivalent to tie-point 2 in Voigt et al. (2012), at 66.52 Ma (Batenburg et al. 2012); 3) the $\delta^{13}C$ minimum within a broad plateau of high $\delta^{13}C$ values in the mid-Maastrichtian, within C31n, at 68.56 Ma (Batenburg et al. 2012); 4) the last $\delta^{13}C$ minimum associated with the Campanian/Maastrichtian Boundary event, followed by a rise in $\delta^{13}C$ values, within C31r. This lowermost tie-point is equivalent to tie-point 6 in Voigt et al. (2012), who assigned it an age of 70.58 Ma. Site U1403 has been plotted on its own, independently-derived astrochronology. Variations in $\delta^{13}C$ values at Shatsky Rise have a similar range as the Site U1403 values, with a minimum value of 2.46‰VPDB in the 405-kyr minimum prior to the K/Pg boundary and maximum values of 3.14‰ in the mid-Maastrichtian, both before and after the negative excursion of the MME. The $\delta^{13}C$ values from Gubbio are lower, but have a similar amplitude with a minimum value of 1.98‰ in the early Maastrichtian and a maximum value of 2.67‰ in the mid-Maastrichtian at 69.0 Ma. The range in $\delta^{13}C$ values of less than 1‰ within records from Site U1403, Site 1210B (Shatsky Rise) and Gubbio stands in contrast to the bulk carbonate $\delta^{13}C$ values from the Zumaia section in northern Spain (Batenburg et al. 2012; Fig. 7). For the Zumaia succession, rhythmic lithological alternations form the basis of a cyclostratigraphic framework, tested by statistical analyses of high-resolution magnetic susceptibility and color reflectance data (Batenburg et al.

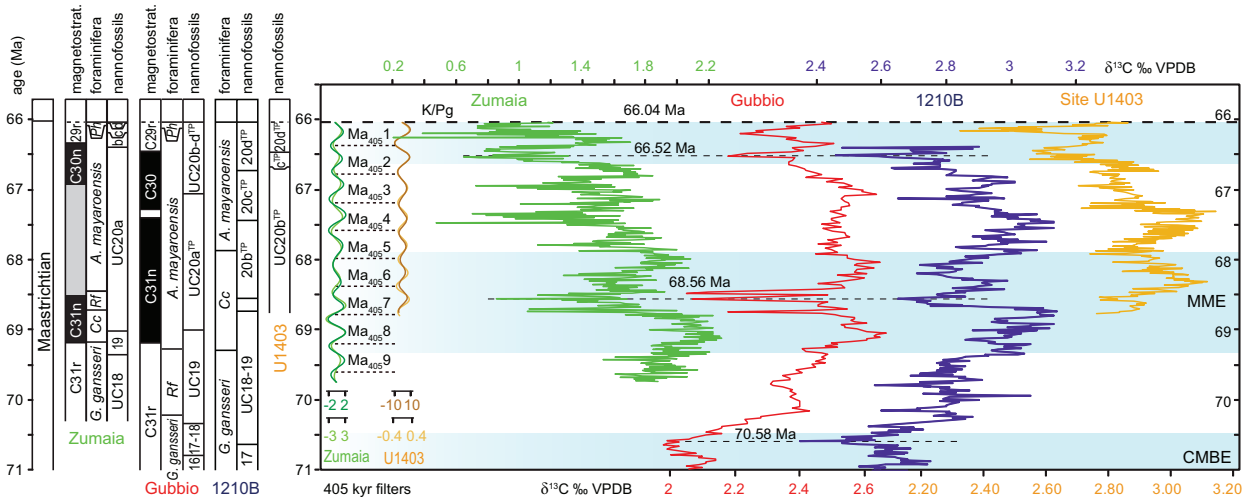

Fig. 7. Correlation of carbon isotope values from IODP Site U1403 (right) with, from left to right, the $\delta^{13}C$ record of the Zumaia section (Batenburg et al. 2012), the Gubbio section in the Umbria–March Basin of Italy (Voigt et al. 2012) and Hole 1210B on Shatsky Rise in the equatorial Pacific Ocean (Jung et al. 2012), with available bio- and magnetostratigraphic data. The records of Site U1403 and Zumaia are plotted against the age models derived from the independently established cyclostratigraphic interpretations for both sections (this study and Batenburg et al. 2014). The 405-kyr band-pass filters of magnetic susceptibility of Zumaia (dark green, bandwidth 300–623 kyr) and Site U1403 (brown, bandwidth 313–627 kyr) are depicted at the left-hand side of the panel, as well as the 405-kyr bandpass filters of color reflectance of Zumaia (light green, bandwidth 300–623 kyr) and ln(Fe/Ca) of Site U1403 (light orange, bandwidth 302–618 kyr). Ma_{405} numbers follow the nomenclature of Husson et al. (2011). The records of Hole 1210B and Gubbio are correlated with the indicated tie-points, using an age of 66.04 for the K/Pg boundary (Renne et al. 2014) and following the age model of Batenburg et al. (2012) for the two late Maastrichtian tie-points and the age-model of Voigt et al. (2012) to derive the age of the lowermost, early Maastrichtian tie-point. Blue bands indicate global carbon isotope oscillations of the Campanian–Maastrichtian boundary event (CMBE), the mid-Maastrichtian event (MME) and the event prior to the K/Pg boundary.

2012). Compared to the carbon isotope data of Site U1403, the Zumaia record shows large (~1‰) variations with a total range of 2‰ over the last 3 Ma of the Maastrichtian (Fig. 7). This variability likely reflects the influence of regional processes such as weathering, runoff and productivity, which may have caused greater temporal changes in the sources of the carbon entering the relatively restricted Basque–Cantabric basin and caused short-term variations superimposed on long-term global trends. The relatively low amplitude variations of bulk carbon isotope values from Site U1403 (up to 0.4‰; Figs. 2, 7) are typical for open ocean settings like the Tethys (Voigt et al. 2012, Sprovieri et al. 2013), the tropical Pacific (Sites 305 and 1210, Voigt et al. 2010, Jung et al. 2012) and the Indian Ocean (Site 762; Thibault et al. 2012a).

The carbon isotope records from Site U1403 and Zumaia show an overall decreasing trend through the late Maastrichtian. Markedly low values near the base of the U1403 record coincide with the Mid-Maastrichtian Event at 68.6 Ma, which can also be observed in the records from Zumaia, Hole 1210B and Gubbio. Distinct oscillations can be observed in all records over an 800-kyr year interval prior to the K/Pg boundary. In between these coeval shifts, the Zumaia record displays a negative shift around 67.5 Ma, which may be related to a relative drop in sea level (Batenburg et al. 2012). In addition, discrepancies between the carbon isotope records may be caused by stratigraphic gaps or flaws in chronology, and require evaluation with independent stratigraphic information, such as bio- and magnetostratigraphy. The behavior of the carbon isotope record of Site U1403 shows most similarity to the oscillations in records from other open-ocean sites, in particular the $\delta^{13}C$ record from Hole 1210B in the Pacific, and is thus likely to be representative of changes in the global carbon cycle. This interpretation is supported by a comparison of available nannofossil marker species. At Site U1403, shipboard calcareous nannofossil biostratigraphy indicates zones UC20b^{TP} to UC20d^{TP} (Norris et al. 2014). Boundaries between these zones are at ~66.68 Ma (base *Ceratolithoides kamptneri*) and ~66.47 Ma (base *Micula prinsii*) if the astronomical age model herein established is applied.

These estimated ages for the nannofossil biozones are somewhat older than ages of the same events at Zumaia (Batenburg et al. 2014). However, diachroneity has been noted in *M. prinsii*, with Boreal appearances typically occurring later (see Gradstein et al. 2012, notes). At ODP Site 762C, Thibault et al. (2012a) reported‘ the first occurance of *M. prinsii* towards the base of magneotochron C29r (66.39 Ma) and Thibault et al. (2016b) report a range of *M. prinsii* ages from 66.2–67 Ma, but mostly towards the younger end of the range, which is generally in good agreement with the estimated age of this study. For *C. kamptneri*, diachroneity has been observed as well, ranging from the base of magnetochron C30n in the Atlantic (e. g., Self-Trail 2001, Thibault and Gardin 2007) to the middle of magnetochron C30n in the central Pacific and Indian Ocean (Thibault and Gardin 2010, Thibault et al. 2012a). An assessment of the planktonic foraminifera biostratigraphy is hampered by the paucity of planktonic foraminifera preserved in these sections (Norris et al. 2014).

Although Site U1403 and the Zumaia section represent markedly different depositional settings, their carbon isotope curves display broadly similar trends when plotted on independent age models. Differences between the curves can be used to identify global versus regional controls on bulk carbonate $\delta^{13}C$. This highlights the utility of carbon isotopes for improving stratigraphic timescales in the latest Cretaceous and their potential to unravel the underlying causes and trigger mechanisms of paleoclimatic and paleoceanographic events.

4. Conclusions

Based on our high-resolution XRF core scanning data of Site U1403, we propose a small correction of the shipboard splice and establish a new astronomically calibrated chronology for the late Maastrichtian interval of this North Atlantic, open ocean site. Time series analyses of elemental and physical property data reveal a hierarchy of cycles, likely reflecting the influence of eccentricity-modulated precession and obliquity. The data records were cut at two levels to accommodate shifts in sedimentation rate, an interpretation supported by changes in the spacing of dark bands. Minima in the ln(Fe/Ca) record are correlated to minima in the stable 405-kyr periodicity of eccentricity. The investigated interval encompasses seven 405-kyr cycles ($Ma_{405}1$ to $Ma_{405}7$), spanning 2.8 Myr from 68.8 to 66.0 Ma. Our new high-resolution stable carbon isotope record from Site U1403 (IODP Expedition 342, Newfoundland Margin) shows distinct variations, including the Mid-Maastrichtian Event and the oscillations prior to the K/Pg boundary. These trends can be correlated to open-ocean carbon isotope records from the Tethyan and Pacific realms, as well as to the hemipelagic Zumaia section in northern Spain. Our study represents the first effort to compare high-resolution Cretaceous $\delta^{13}C$ records from different localities that have independent, high-resolution astrochronologies. Comparison of carbon isotope stratigraphies from open-ocean and hemipelagic settings adds insights into regional versus global drivers of $\delta^{13}C$ variations in marine sediments. The amplitude of carbon isotope variation at Zumaia is significantly higher than at Site U1403, indicating a strong influence of regional processes on the carbon isotope signal in the marginal Basque-Cantabric basin. In contrast, the Site U1403 record displays typical open ocean values when compared to the Tethyan record of Gubbio and the Pacific record of Site 1210B. Site U1403 offers great promise as a potential reference section for studying paleoclimatic and paleoceanographic change during the latest Cretaceous.

Acknowledgements. This research used samples provided by the Integrated Ocean Drilling Program (IODP), which is sponsored by the U.S. National Science Foundation and participating countries under management of Joint Oceanographic Institutions, Inc. This research used data acquired at the XRF Core Scanner Lab at the MARUM-Center for Marine Environmental Sciences, University of Bremen, Germany. Sven Hofmann is thanked for laboratory assistance. Dominik Leonhardt helped with processing of sediment samples. We would like to thank Nicolas Thibault, Helmut Weissert, and two anonymous reviewers for comments on an earlier version of the manuscript. Funding for this study was provided by the DFG to O. F. (Emmy Noether research group “Meso- and Cenozoic paleoceanography”; grant FR2544/2-1 and grant FR2544/5) and to S. V. (DFG grant VO 687/14-1). The bulk carbon isotope and oxygen isotope data, as well as the Si, Ca, Fe and Ba counts from XRF analyses, are available in the Pangaea database (doi. pangaea.de/10.1594/PANGAEA.875743).

References

Anderson, T. F., Arthur, M. A., 1983. Stable isotopes of oxygen and carbon and their application to sedimentologic and paleoenvironmental problems. In: Arthur, M. A., Anderson, T. F., Kaplan, I. R. V. J., Land, L. S. (Eds.): Stable Isotopes in Sedimentary Geology. Society of Economic Paleontologists and Mineralogists, Dallas, pp. 1–151.

Barrera, E., 1994. Global environmental changes preceding the Cretaceous–Tertiary boundary: Early–Late Maastrichtian transition. Geology 22, 877–880.

Barrera, E., Savin, S.M., 1999. Evolution of late Campanian-Maastrichtian marine climates and oceans. Geological Society of America Special Papers 332, 245–282.

Barrera, E., Savin, S.E., Thomas, E., Jones, C.E., 1997. Evidence for thermohaline-circulation reversals controlled by sea-level change in the latest Cretaceous. Geology 25, 715–718.

Batenburg, S.J., Sprovieri, M., Gale, A.S., Hilgen, F.J., Hüsing, S., Laskar, J., Liebrand, D., Lirer, F., Orue-Etxebarria, X., Pelosi, N., Smit, J., 2012. Cyclostratigraphy and astronomical tuning of the Late Maastrichtian at Zumaia (Basque country, Northern Spain). Earth and Planetary Science Letters 359–360, 264–278.

Batenburg, S.J., Gale, A.S., Sprovieri, M., Hilgen, F.J., Thibault, N., Boussaha, M., Orue-Etxebarria, X., 2014. An astronomical time scale for the Maastrichtian based on the Zumaia and Sopelana sections (Basque country, northern Spain). Journal of the Geological Society 171, 165–180.

Bornemann, A., Norris, R.D., Friedrich, O., Beckmann, B., Schouten, S., Sinninghe Damsté, J., Vogel, J., Hofmann, P., Wagner, T., 2008. Isotopic evidence for glaciation during the Cretaceous supergreenhouse. Science 319, 189–192.

Burnett, J.A. 1998. Upper Cretaceous, in Calcareous nannofossil biostratigraphy. In: Bown, P.R. (Eds.): Chapman and Hall, London, pp. 132–199.

Clarke, L.J., Jenkyns, H.C., 1999. New oxygen-isotope evidence for long-term Cretaceous climate change in the Southern Hemisphere. Geology 27, 699–702.

Expedition 342 Scientists, 2012. Paleogene Newfoundland sediment drifts. Integrated Ocean Drilling Program Preliminary Report 342. doi:10.2204/iodp.pr.342.2012.

Forster, A., Schouten, S., Baas, M., Sinninghe Damsté, J., 2007. Mid-Cretaceous (Albian–Santonian) sea surface temperature record of the tropical Atlantic Ocean. Geology 35, 919–922.

Frank, T.D., Arthur, M.A., 1999. Tectonic Forcings of Maastrichtian Ocean-Climate Evolution. Paleoceanography 14, 103–117.

Frank, T.D., Thomas, D.J., Leckie, R.M., Arthur, M.A., Bown, P.R., Jones, K., Lees, J.A., 2005. The Maastrichtian record from Shatsky Rise (northwest Pacific): A tropical perspective on global ecological and oceanographic changes. Paleoceanography 20, doi:10.1029/2004PA001052.

Friedrich, O., Hemleben, C., 2007. Early Maastrichtian benthic foraminiferal assemblages from the western North Atlantic (Blake Nose) and their relation to paleoenvironmental changes. Marine Micropaleontology 62, 31–44.

Friedrich, O., Reichelt, K., Herrle, J.O., Lehmann, J., Pross, J., Hemleben, C., 2003. Formation of the Late Aptian Niveau Fallot black shales in the Vocontian Basin (SE France): evidence from foraminifera, palynomorphs, and stable isotopes. Marine Micropaleontology 49, 65–85.

Friedrich, O., Herrle, J.O., Kößler, P., Hemleben, C., 2004. Early Maastrichtian stable isotopes: changing deep water sources in the North Atlantic? Palaeogeography, Palaeoclimatology, Palaeoecology 211, 171–184.

Friedrich, O., Erbacher, J., Moriya, K., Wilson, P.A., Kuhnert, H., 2008. Warm saline intermediate waters in the Cretaceous tropical Atlantic Ocean. Nature Geoscience 1, 453–457.

Friedrich, O., Herrle, J.O., Wilson, P.A., Cooper, M.J., Erbacher, J., Hemleben, C., 2009. Early Maastrichtian carbon cycle perturbation and cooling event: Implications from the South Atlantic Ocean. Paleoceanography 24, PA2211, doi:10.1029/2008PA001654.

Friedrich, O., Norris, R.D., Erbacher, J., 2012. Evolution of middle to Late Cretaceous oceans-A 55 m.y. record of Earth's temperature and carbon cycle. Geology 40, 107–110.

Gradstein, F.M., Ogg, J.G., Schmitz, M.D., Ogg, G.M. (Eds.), 2012. The Geologic Time Scale 2012. Boston, USA, Elsevier, 2 volumes plus chart, 1176 pp.

Grinsted, A., Moore, J.C., Jevrejeva, S., 2004. Application of the cross wavelet transform and wavelet coherence to geophysical time series. Nonlinear Processes in Geophysics 11, 561–566.

Henehan, M.J., Hull, P.M., Penman, D.E., Rae, J.W., Schmidt, D.N., 2016. Biogeochemical significance of pelagic ecosystem function: an end-Cretaceous case study. Philosophical Transactions of the Royal Society B, 371(1694), doi:10.1098/rstb.2015.0510.

Huber, B.T., Watkins, D.K., 1992. Biogeography of Campanian–Maastrichtian calcareous plankton in the region of the Southern Ocean: paleogeographic and paleoclimatic implications. Antarctic Research Series 56, 31–60.

Huber, B.T., Norris, R.D., MacLeod, K.G., 2002. Deep-sea paleotemperature record of extreme warmth during the Cretaceous. Geology 30, 123–126.

Husson, D., Galbrun, B., Laskar, J., Hinnov, L.A., Thibault, N., Gardin, S., Locklair, R.E., 2011. Astronomical calibration of the Maastrichtian (Late Cretaceous). Earth and Planetary Science Letters 305, 328–340.

Jenkyns, H.C., Gale, A.S., Corfield, R.M., 1994. Carbon-isotope and oxygen-isotope stratigraphy of the English Chalk and Italian Scaglia and its palaeoclimatic significance. Geological Magazine 131, 1–34.

Jung, C., Voigt, S., Friedrich, O., 2012. High-resolution carbon-isotope stratigraphy across the Campanian-Maastrichtian boundary at Shatsky Rise (tropical Pacific). Cretaceous Research 37, 177–185.

Jung, C., Voigt, S., Friedrich, O., Koch, M.C., Frank, M., 2013. Campanian-Maastrichtian ocean circulation in the tropical Pacific. Paleoceanography 28, 562–573.

Kirtland-Turner, S., Sexton, P.F., Charles, C., Norris, R., 2014. Persistence of carbon release events through the peak of early Eocene global warmth. Nature Geoscience 7, 748–751.

Kuiper, K.F., Deino, A., Hilgen, F.J., Krijgsman, W., Renne, P.R., Wijbrans J.R., 2008. Synchronizing Rock Clocks of Earth History. Science 320, 500–504.

Laskar, J., Gastineau, M., Delisle, J.-B., Farrés, A., Fienga, A., 2011. Strong chaos induced by close encounters with Ceres and Vesta. Astronomy and Astrophysics 532, L4.

Lees, J.A., 2002. Calcareous nannofossil biogeography illustrates palaeoclimate change in the Late Cretaceous Indian Ocean. Cretaceous Research 23, 537–634.

Lees, J.A., Bown, P.R., 2005. Upper Cretaceous calcareous nannofossil biostratigraphy, ODP Leg 198 (Shatsky Rise, northwest Pacific Ocean). Proceedings of the Ocean Drilling Program Scientific Results 198, 1–60.

Li, L., Keller, G., 1998. Maastrichtian climate, productivity and fauna1 turnovers in planktic foraminifera in South Atlantic DSDP sites 525A and 21. Marine Micropaleontology 33, 55–86.

Liebrand, D., de Bakker, A.T., Beddow, H.M., Wilson, P.A., Bohaty, S.M., Ruessink, G., Pälike, H., Batenburg, S.J., Hilgen, F.J., Hodell, D.A., Huck, C.E., 2017. Evolution of the early Antarctic ice ages. Proceedings of the National Academy of Sciences, p.201615440.

MacLeod, K.G., 1994. Bioturbation, inoceramid extinction and mid Maastrichtian ecological change. Geology 22, 139–142.

MacLeod, K.G., Huber, B.T., Ward, P.D., 1996. The biostratigraphy and paleobiogeography of Maastrichtian inoceramids. Geological Society of America Special Papers 307, 361–373.

MacLeod, K.G., Londono, C.I., Martin, E.E., Berrocoso, A.J., Basak, C., 2011. Changes in North Atlantic circulation at the end of the Cretaceous greenhouse interval. Nature Geoscience 4, 779–782.

Marshall, J.D., 1992. Climatic and oceanographic isotopic signals from the carbonate rock record and their preservation. Geological Magazine 129, 143–160.

Moriya, K., Goto, A.S., Hasegawa, T., 2012. Stable carbon and oxygen isotope analyses of carbonate using a continuous flow isotope ratio mass spectrometry. The science reports of the Kanazawa University 56, 45–58.

Norris, R.D., Wilson, P.A., Blum, P., Expedition 342 Scientists, 2014. Paleogene Newfoundland Sediment Drifts and MDHDS Test. Proceedings of the Integrated Ocean Drilling Program 342, Integrated Ocean Drilling Program, College Station, TX, doi:10.2204/iodp.proc.342.2014.

Paillard, D., Labeyrie, L., Yiou, P., 1996. Macintosh program performs timeseries analysis. EOS Transactions 77, 379–397.

Premoli Silva, I., Sliter, W.V., 1994. Cretaceous planktonic foraminiferal stratigraphy and evolutionary trends from the Bottacione section, Gubbio, Italy. Paleontographica Italica 82, 1–89.

Renne, P.R., Deino, A.L., Hilgen, F.J., Kuiper, K.F., Mark, D.F., Mitchell, W.S., Morgan, L.E., Mundil, R., Smit, J., 2013. Time scale of critical events around the Cretaceous-Paleogene boundary. Science 339, 684–687.

Robinson, S.A., Vance, D., 2012. Widespread and synchronous change in deep-ocean circulation in the North and South Atlantic during the Late Cretaceous. Paleoceanography 27, PA1102, doi:10.1029/2011PA002240.

Scholle, P.A., Arthur, M.A., 1980. Carbon isotope fluctuations in Cretaceous pelagic limestones: potential stratigraphic and petroleum exploration tool. AAPG Bulletin 64 (1), 67–87.

Schrag, D.P., DePaolo, D.J., Richter, F.M., 1995. Reconstructing past sea surface temperatures: Correcting for diagenesis of bulk marine carbonate. Geochimica et Cosmochimica Acta 59, 2265–2278.

Schulz, M., Mudelsee, M., 2002. REDFIT: estimating red-noise spectra directly from unevenly spaced paleoclimatic time series. Computers & Geosciences 28, 421–426.

Sprovieri, M., Sabatino, N., Pelosi, N., Batenburg, S.J., Coccioni, R., Iavarone, M., Mazzola, S., 2013. Late Cretaceous orbitally-paced carbon isotope stratigraphy from the Bottaccione Gorge (Italy). Palaeogeography, Palaeoclimatology, Palaeoecology 379, 81–94.

Thibault, N., Gardin, S., 2007. The late Maastrichtian nannofossil record of climate change in the South Atlantic DSDP Hole 525A. Marine Micropaleontology 65, 163–184.

Thibault, N., Gardin, S., 2010. The calcareous nannofossil response to the end-Cretaceous warm event in the Tropical Pacific. Palaeogeography, Palaeoclimatology, Palaeoecology 291, 239–252.

Thibault, N., Husson, D., Harlou, R., Gardin, S., Galbrun, B., Huret, E., Minoletti, F., 2012a. Astronomical calibration of upper Campanian–Maastrichtian carbon isotope events and calcareous plankton biostratigraphy in the Indian Ocean (ODP Hole 762C): Implication for the age of the Campanian–Maastrichtian boundary. Palaeogeography, Palaeoclimatology, Palaeoecology 337–338, 52–71.

Thibault, N., Harlou, R., Schovsbo, N., Schioler, P., Lauridsen, B.W., Sheldon, E., Stemmerik, L., Surlyk, F., 2012b. Upper Campanian–Maastrichtian carbon-isotope stratigraphy of the Danish Basin: calibration with calcareous nannofossil and dinoflagellate events in the Boreal Realm. Cretaceous Research 33, 72–90.

Thibault, N., Harlou, R., Schovsbo, N.H., Stemmerik, L., Surlyk, F., 2016a. Late Cretaceous (late Campanian–Maastrichtian) sea-surface temperature record of the Boreal Chalk Sea. Climate of the Past 12, 429–438.

Thibault, N., Galbrun, B., Gardin, S., Minoletti, F., Le Callonnec, L., 2016b. The end-Cretaceous in the southwestern Tethys (Elles, Tunisia): orbital calibration of paleoenvironmental events before the mass extinction. International Journal of Earth Sciences 105, 771–795.

Thierstein, H.R., Roth, P.H., 1991. Stable isotopic and carbonate cyclicity in Lower Cretaceous deep-sea sediments: dominance of diagenetic effects. Marine Geology 97 (1–2), pp.1–34.

Voigt, S., Wiese, F., 2000. Evidence for Late Cretaceous (late Turonian) climate cooling from oxygen-isotope variations and palaeobiogeographic changes in Western and Central Europe. Journal of the Geological Society 157, 737–744.

Voigt, S., Friedrich, O., Norris, R.D., Schönfeld, J., 2010. Campanian–Maastrichtian carbon isotope stratigraphy: shelf-ocean correlation between the European shelf sea

and the tropical Pacific Ocean. Newsletters on Stratigraphy 44, 57–72.

Voigt, S., Gale, A. S., Jung, C., Jenkyns, H. C., 2012. Global correlation of Upper Campanian–Maastrichtian successions using carbon-isotope stratigraphy: development of a new Maastrichtian timescale. Newsletters on Stratigraphy 45, 25–53.

Voigt, S., Jung, C., Friedrich, O., Frank, M., Teschner, C., Hoffmann, J., 2013. Tectonically restricted deep-ocean circulation at the end of the Cretaceous greenhouse. Earth and Planetary Science Letters 369–370, 169–177.

Weissert, H., Joachimski, J., Sarnthein, M, 2008. Chemostratigraphy. Newsletters on Stratigraphy 42, 145–179.

Weltje, G. J., Tjallingii, R., 2008. Calibration of XRF core scanners for quantitative geochemical logging of sediment cores: theory and application. Earth and Planetary Science Letters 274, 423–438.

Westerhold, T., Röhl, U., Raffi, I., Fornaciari, E., Monechi, S., Reale, V., Bowles, J., Evans, H. F., 2008. Astronomical calibration of the Paleocene time. Palaeogeography, Palaeoclimatology, Palaeoecology 257, 377–403.

Wilf, P., Johnson, K. R., Huber, B. T., 2003. Correlated terrestrial and marine evidence for global climate changes before mass extinction at the Cretaceous–Paleogene boundary. Proceedings of the National Academy of Sciences 100 (2), 599–604.

Wilson, P. A., Norris, R. D., Cooper, M. J., 2002. Testing the Cretaceous greenhouse hypothesis using glassy foraminiferal calcite from the core of the Turonian tropics on Demerara Rise. Geology 30, 607–610.

Manuscript received: January 31, 2017
Revised version accepted: May 24, 2017